Proceedings of the ASME 2020
Dynamic Systems and Control Conference
DSCC2020
October 4-7, 2020, Pittsburgh, Pennsylvania, USA

Paper 24598

CHARACTERIZATION OF DUTY CYCLES FOR THE PEAK SHAVING ELECTRIC GRID ENERGY STORAGE APPLICATION

Kevin Moy, Seong Beom Lee, and Simona Onori

Stanford University, Department of Energy Resource Engineering, Stanford, CA 94305, USA

ABSTRACT

Energy storage systems (ESSs), such as lithium-ion batteries, are being used today in renewable grid systems to provide the capacity, power, and quick response required for operation in grid applications, including peak shaving, frequency regulation, back-up power, and voltage support. Each application imposes a different duty cycle on the ESS. This represents the charge/discharge profile associated with energy generation and demand. Different duty cycle characteristics can have different effects on performance, life, and duration of ESSs. Within lithium-ion batteries, various chemistries exist that own different features in terms of specific energy, power and cycle life, that ultimately determine their usability and performance. Therefore, characterization of duty cycles is key to determine how to properly design lithium-ion battery system for grid applications. Given the usage-dependent degradation trajectories, this research task is a critical step to study the unique aging behaviors of grid batteries. Significant energy and cost savings can be achieved by the optimal application of lithium-ion batteries for grid energy storage, enabling greater utilization of renewable grid systems. In this paper, we identify a systematic approach, based on the adoption of both unsupervised learning and frequency domain techniques, to characterizing grid-specific duty cycles for the grid-specific peak shaving application.

1. INTRODUCTION

In 2019, global renewable generation capacity reached 2,179 gigawatts [1]. While hydropower remains the largest contributor to renewable generation, the fastest-growing resources are photovoltaic and wind power, accounting for 90% of all net renewable capacity additions in 2019. These resources comprise a substantial amount of the grid generation power. In California, for example, variable renewable generation (i.e. wind and solar power) constituted 29% of the total generation in 2019 [2]. The introduction of these intermittent generation sources poses challenges to conventional methods for planning the daily operation of the electric grid. Additionally, the diurnal availability of solar generation can aggravate ramping problems when load increases as solar production decreases. This is problematic in grids with high solar penetration; in the California independent system operator (ISO), this has been termed the "duck curve" [3]. Energy storage systems (ESSs) are considered as a way to address the aforementioned drawbacks. Among many other technologies for ESSs, electrochemical energy storage devices are the main ones implemented and used today for grid services, of which nearly 80% is provided by lithium-ion batteries since 2003 [4, 5].

1.1 Motivation

Lithium-ion batteries are prevalent in renewable grid systems as ESSs since they can provide fast response time, modularity, flexible installation, and short construction cycles [6]. ESSs in renewable grid systems participate in grid applications, such as peak shaving, frequency regulation, voltage support, and back-up power, supporting grid operations at various locations on the grid [7]. However, battery degradation resulting from participation in grid applications is considered a major factor for profitable operation [8]. The degradation trajectories of lithium-ion battery systems depend both on the particular lithium-ion chemistry of the battery, and the usage within these grid applications. Current battery technology accounts for various lithium-ion chemistries, each with different characteristics that may be appropriate for different use within the grid needs. For example, a chemistry with high specific energy but low cycle life may be appropriate for back-up power, as this application only uses the battery during grid outages for extended multi-hour durations [9]. Therefore, properly assessing the most appropriate chemistry for a targeted application can maximize the performance, usability, and duration of entire grid systems.

The usage within each grid application is characterized by duty cycles. A duty cycle is a charge and discharge profile (given in terms of power or current) representing the demands associated with a specific grid application. Likewise, each grid application has different duty cycling characteristics, which can lead to different capacity fade trends in battery systems. Understanding degradation mechanisms triggered by characteristic grid-specific duty cycles is key to develop predictive tools that can be integrated into cost/benefit analyses to maximize revenue and minimize lost capacity. It is well known that differences in duty cycles could significantly impact the durability of ESSs [10]. As the duty cycles and operating conditions can be vastly different for stationary grid-scale

storage as opposed to automotive energy storage devices, predictive ESS models properly calibrated over grid-specific duty cycles are missing in today's literature. It is imperative to understand and predict the performance and durability of large grid-level battery ESSs which calls for the study and analysis of actual duty cycles for each application.

In current practice, a plethora of work has been conducted on the analysis and characterization of duty cycles for automotive batteries. In [11], real driving cycles for hybrid electric vehicles were analyzed by distribution histogram. In [12], a way of creating effective synthetic duty cycles was published based on pulse-multisine design technique where a Discrete Fourier Transform (DFT) approach was adopted to show that the pulse power current duty cycle was insufficient to characterize the amplitude and frequency bandwidth of a real driving cycle. In [13], real battery duty cycles were categorized by driving speed and style, and an approach based on the power spectral density (PSD) was applied to each category by differentiating discharge and charge events. In addition, various characterization methods have been proposed for different research purposes, using several analytical techniques [14-16]. In [14], electric bus driving cycles were analyzed using the cross-PSD, involving the DFT of both duty cycles. In [15], high-performance multisine, random pulse, and inverse cumulative distribution analysis were used to characterize duty cycles of large-format automotive lithium-ion pouch cells. In [16], a signal design method was proposed to identify battery model parameters using frequency range analysis of actual driving cycles.

Current studies in renewable grid applications show the lack of a systematic approach to define characteristic grid-specific duty cycles. For example, Sandia National Laboratory has previously created a methodology for testing the performance of energy storage, using duty cycles under various grid applications, including peak shaving, frequency regulation, PV smoothing, and solar firming [17]. However, these duty cycles are generated directly from existing data, with minimal characterization of the duty cycles under this existing data. For PV smoothing, ESS duty cycles were generated from existing PV generation profiles, without identification of characteristic duty cycles [18]. For frequency regulation, PSD was used as exploratory analysis of the dispatch signal, but ultimately was not used in duty cycle construction; "aggressive" and "average" days from the dispatch were used instead [19].

In other studies, performance and life of stationary battery systems were investigated, including performance under frequency regulation given different dispatch methodologies [20], and energy arbitrage [8]. These studies adopted simplistic empirical models for battery degradation and predicted performance, and simulated battery degradation directly from the dispatch profiles, without characterizing the dispatch.

In this paper, we first determine characteristic duty cycles using *k-means* clustering for the grid application of peak shaving. We then use the PSD to extract and analyze the frequency content of the clustered duty cycles. The two points above are instrumental for analyzing how grid-batteries are operated under this application, and can be used to study the unique performance and aging behaviors of batteries in this *modus operandi*.

There are four sections in this paper: peak shaving, methodology, data description, and duty cycle analysis. In the peak shaving section, we study and discuss the motivation for and operation of peak shaving, and how battery ESSs are used to support such a grid application. In the methodology section, we describe in detail fast Fourier transform (FFT), PSD, and k-means clustering, and their relevance to duty cycle analysis. In the data description section, we present the data used for the characterization and synthesis of duty cycles. In the duty cycle analysis section, we present a method for duty cycle characterization and apply this process to different peak shaving dispatches, and compare them to electric vehicle duty cycles. Concluding remarks are found in the conclusion section.

2. PEAK SHAVING

The electric utility supplies electricity from the grid to meet the demand of an end user's load, e.g., a house, office, or factory. The facility is then billed monthly by the utility, as measured by the utility meter. The bill charges are defined in a tariff rate determined by the utility, and include several elements such as time-of-use charges and demand charges, based on the amount of electric energy and maximum (peak) power consumed from the grid by the load.

Peak shaving is used to lower the monthly peak power consumed by the facility from the grid ("shaving" the peak). Different strategies for peak shaving exist, including reducing peak consumption of facility loads, managing charging of electric vehicles, and dispatching battery ESSs [21]. For batteries, peak shaving is accomplished by discharging when the load is large and charging from the grid when electricity is cheap [22]. Based on peak shaving, the potential market for residential battery ESSs is approximately 5 million end users in the United States [23]. Real-time operation of a battery for peak-shaving can involve simple control loops to discharge or charge the battery based on current power flow from the grid and SOC of the battery [24], or include an optimization algorithm to compute optimum battery dispatch given additional constraints, such as the power flow through grid infrastructure [25].

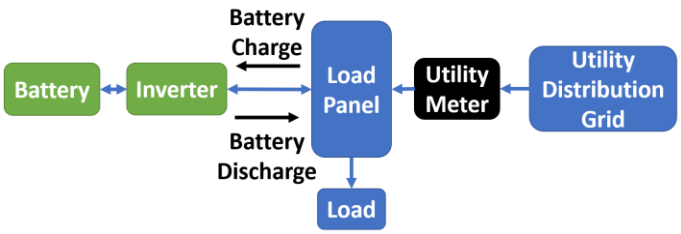

FIGURE 1: PEAK SHAVING POWER FLOW DIAGRAM. Arrows indicate direction of power flow. The battery charges and discharges to offset the load, reducing the power flow as seen by the utility meter, and reducing the utility bill.

3. METHODOLOGY

This section describes the methods and techniques used in this paper to analyze grid application duty cycles.

3.1 Fast Fourier Transform

The FFT method is an algorithm that computes the DFT of a time-series sequence [26]. The DFT takes as input a sequence of values $x[n],\ n = 0, 1, 2, \dots, N-1$ of length N, in time. This sequence is then decomposed into a sequence of sinusoidal components $X[q],\ q = 0, \dots, N-1$, of length N, for different frequencies nq/N.

$$X[q] = \sum_{n=0}^{N-1} x[n] e^{-\frac{i2\pi nq}{N}}, \quad q = 0, \dots, N-1 \qquad (1)$$

As described in Section 4, the dispatch profiles of the battery are recorded as time-series sequences, so the FFT forms the basis for the duty cycle analysis.

3.2 Power spectral density

The PSD is the measure of a signal's power content as a function of its frequency. Our duty cycle analysis uses Welch's method for computing PSD [27]. It is based on the periodogram of the signal, which in turn is based off of the DFT of the signal. Welch's method is summarized as follows: a sequence of values $x[n] = 0, 1, 2, \dots, N-1$, of length N collected at interval periods T, is partitioned into K segments of length M where $M < N - 1$ [28].These segments overlap by an amount S, usually in the range $0.4M \leq S \leq M$.[1]

For each segment $r = 1 \dots R$, represented as the subset $x[m]$ of the signal where $m = (r-1)S, \dots, M + (r-1)S - 1$, a windowed DFT $X_r(f)$ is computed at frequency f with window function[2] w.

$$X_r(f) = \sum_m x[m] w[m] e^{-i2\pi fm} \qquad (4)$$

Then, each segment DFT is used to form the segment's modified periodogram value, $P_r(f)$ as follows:

$$P_r(f) = \frac{1}{\sum_{m=0}^{M} w^2[m]} |X_r(f)|^2 \qquad (5)$$

Finally, the periodogram values are averaged to obtain Welch's estimate of the PSD.

$$S_x(f) = \frac{1}{R} \sum_{r=1}^{R} P_r(f) \qquad (6)$$

We use the `pwelch` function in MATLAB for Welch's method for PSD, which uses a Hamming window as the default window function. In addition to the signal sequence, `pwelch` accepts as parameters frequency f, segment length M, and overlap N. For our analysis, we choose the frequency to be that of the time-series sequence interval ($f = 1/T$) and overlap $N = M/2$, both of which are within the ranges suggested by [28]. Fixing these parameters leaves us with M as the sole degree of freedom, allowing us to determine the amount of smoothing and averaging in Welch's method; as M decreases for fixed N and f, more periodograms are calculated across shorter segments. Throughout this paper, these parameters are set at f = 1/3600 Hz, M = 48, and $N = M/2$ = 24, chosen to balance the tradeoff between smoothing and noise reduction.[3]

By averaging these modified (windowed) periodograms, Welch's method for PSD allows us to study the spectral characteristics of a dataset, removing much of the signal noise retained in the FFT. Figure (2) shows the periodogram of the FFT for the peak shaving dispatch profile, separated by charge and discharge. The PSD for the same dispatch profile is also shown in Figure (13), displaying the same characteristics as the FFT periodogram but with a smoother profile.

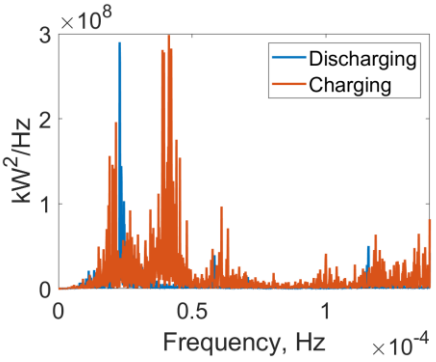

FIGURE 2: PERIODOGRAM FROM FFT FOR PEAK SHAVING YEARLY DISPATCH, "LARGEOFFICENEW" PROFILE. The FFT and its respective periodogram are computed for the charge and discharge dispatch profile separately.

As the degradation and health of the battery are dependent on different mechanisms for charging and discharging, separating these two events in the PSD analysis could give useful insights on the battery usage.

3.3 Mean centering

The battery dispatch for charging and discharging are strictly negative and strictly positive, respectively. Separating the charge and discharge and directly taking the FFT would yield a bias in the FFT periodogram, appearing as low-frequency components not present in the original dispatch. In order to remove this effect, mean centering is applied to ensure that the resulting separated charge and discharge profiles have zero mean, while preserving all frequency components in these profiles.

---

[1] This rule of thumb for selecting overlap S is as presented in [30].

[2] The window function is used to take into account the fact that the segment may not be an exact multiple of a given frequency. The windowing function is greatest in the center of the segment and decreases towards zero at the ends, so that any discontinuities between the beginning and end of the signal are minimized.

[3] The choice of M and N correspond to segments of two days and one day, respectively.

Mean centering is applied to the entire dispatch profile using the following procedure. This procedure is described for obtaining mean-centered discharge (or charge) profiles, below:

1. Construct a new profile consisting of only non-negative (non-positive) dispatch.
2. Find each individual discharge (charge) instance within this new profile, where a discharge (charge) instance is defined as the battery starting at 0 dispatch, positively (negatively) dispatching, then returning to 0 dispatch.
3. Construct a new mean-centered discharge (charge) profile by concatenating each discharge (charge) instance with a copy of reversed sign.

3.4 k-means clustering

Clustering is an unsupervised learning method to organize and partition data into "clusters". Data within each cluster share some features [29]. This class of methods has been widely studied for characterizing time-series data [30].

In k-means clustering, k clusters are constructed from n observations of data, where each observation is assigned a cluster by the closest Euclidean distance to the cluster centroid, or the mean value of all observations in the cluster. That is, given k desired clusters, and dataset of observations $x_1 \dots x_n$, k-means clustering determines k cluster centroids as a solution $\phi^* = [c_1 \dots c_k]^T$ that minimizes the cost function J, below [31]:

$$\phi^* = \min J, \tag{7}$$

$$J = \sum_{i=1}^{n} \min_{j=1\dots k} \|x_i - c_j\|^2 \tag{8}$$

We use the `kmeans` function in MATLAB to apply k-means clustering to the dispatch profiles. As the initialization of the cluster centroids is important for clustering convergence, the `k-means++` algorithm is used for this initialization [31]. Within the context of electric power systems, k-means clustering has been applied to solar and wind generation profiles [32, 33], electricity load demand profiles [34, 35], and driving cycles for electric vehicles [36]. This paper represents the first application of k-means clustering to grid storage battery dispatch profiles. The application of k-means clustering to the dataset is as follows. We first choose each observation to represent one day, reshaping the time-series data into an array where each row is the dispatch for one day, and each column is the dispatch for one hour within the day. Next, as some days contain zero dispatch (i.e. no charging or discharging of the battery), the corresponding rows of the array are removed. Days with missing or corrupted values (e.g. NaN) are also removed. The number of clusters, k, is then chosen, and k-means clustering is applied to the remaining nonzero dispatch array.

The output of k-means clustering on the dispatch data is k "cluster centroids", representing the average daily dispatch within each cluster, and cluster assignments for each nonzero dispatch day.

4. DATA DESCRIPTION

The time-series dispatch profiles for the grid application are summarized in Table (1).

TABLE 1: GRID APPLICATION DISPATCH DATA SOURCES.

Application	System Rated Power, kW	System Rated Energy, kWh	Load Name	Tariff Rate
Peak Shaving	200	400	LargeOfficeNew	PG&E E19
			SuperMarketNew	PG&E A10

Peak shaving data were obtained from a publicly-available optimization and simulation tools for energy storage: QuESt, developed by Sandia National Laboratories [37]. QuESt allows users to select facility load profiles, energy storage parameters such as rated power and energy, as well as a tariff rate structure. QuESt then uses this input data to simulate the energy storage dispatch per month over one year, optimizing the dispatch for bill reduction by peak shaving. This dispatch data is obtained as an hourly dispatch (frequency 1/3600 Hz).

Figure (3) shows the QuESt-simulated dispatch of the 200kW, 400kWh battery using the "LargeOfficeNew" load over the year. The histogram at the left in Figure (4) shows a bias towards high power charging of the battery. The histogram at the right in Figure (4) also shows that when the battery is at rest (i.e. neither charging nor discharging), the majority of rest instances are less than 48 hours in length, with most rest instances between 10 and 20 hours long. These rest instances are periods of time when the battery is not actively used for peak shaving, and indicate opportunities to employ the batteries for other grid applications during these periods.

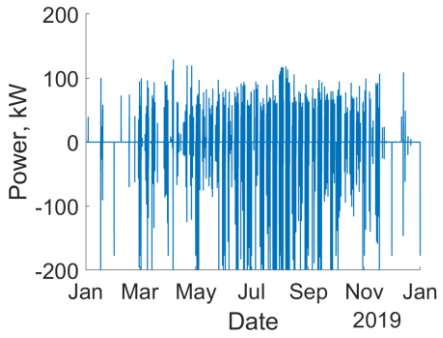

FIGURE 3: YEARLY DISPATCH OF A 200kW, 400kW GRID STORAGE BATTERY FOR PEAK SHAVING, "LARGEOFFICENEW" PROFILE. The QuESt tool was used to produce this dispatch, which QuESt simulated on an hourly basis. Discharging is positive, while charging is negative.

Figure (5) shows the QuESt-simulated dispatch of the 200kW, 400kWh battery using the "SuperMarketNew" load over the year. Figure (6) is the histogram of nonzero dispatch over the year for the "SuperMarketNew" load, showing that there is both a different distribution of charging and discharging, as well as

more frequent dispatch with shorter rest periods, than the "LargeOfficeNew" load.

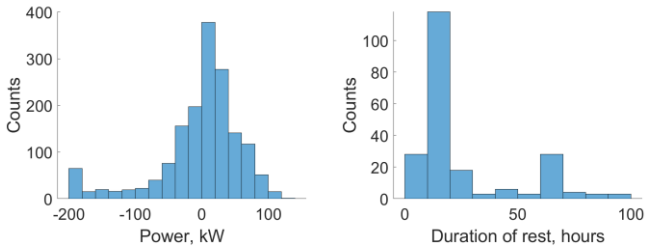

FIGURE 4: LEFT: HISTOGRAM OF NON-ZERO PEAK SHAVING DISPATCH, "LARGEOFFICENEW". Datapoints corresponding to zero dispatch were excluded from this histogram. Histogram shows a bias towards higher charging (negative) power. RIGHT: HISTOGRAM OF REST PERIODS DURING DISPATCH, "LARGEOFFICENEW". The period of rest is determined as the length of time between when a charge or discharge ends, and the next charge or discharge begins.

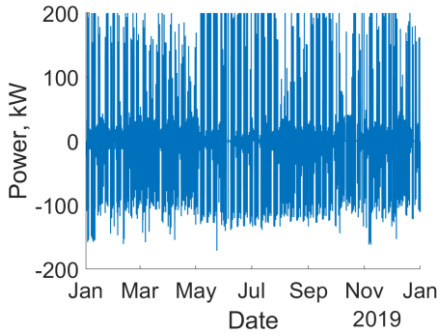

FIGURE 5: YEARLY DISPATCH OF A 200kW, 400kW GRID STORAGE BATTERY FOR PEAK SHAVING, "SUPERMARKETNEW" PROFILE. The QuESt tool was used to produce this dispatch on hourly basis. Discharging is positive and charging is negative.

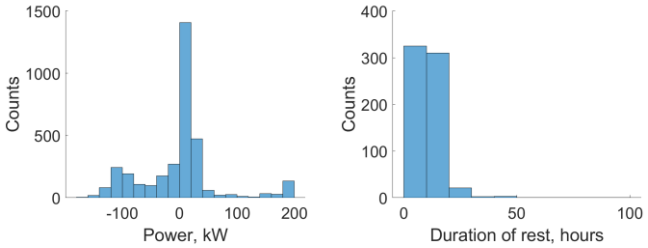

FIGURE 6: LEFT: HISTOGRAM OF NONZERO PEAK SHAVING DISPATCH, "SUPERMARKETNEW". Datapoints corresponding to dispatch of 0 were excluded from this histogram. RIGHT: HISTOGRAM OF REST PERIODS DURING DISPATCH, "SUPERMARKETNEW". The period of rest is determined as the length of time between when a charge or discharge ends, and the next charge or discharge begins.

5. DUTY CYCLE ANALYSIS

For a given grid storage application dispatch profile, we conduct the following steps. First, we use k-means clustering to obtain distinct duty cycle clusters. The number of clusters is chosen to determine duty cycles that represent the range of charging and discharging behavior within the dispatch profile under consideration. Then, within each cluster, we compute the PSD of the charge and discharge separately. This process is summarized in Figure (7).

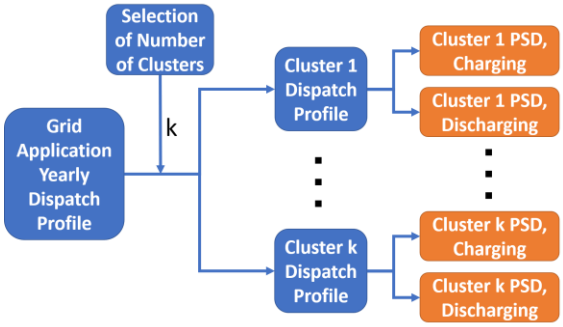

FIGURE 7: FLOW DIAGRAM FOR DUTY CYCLE ANALYSIS. The outputs of this analysis are shown in orange: PSD for charging and discharging within each dispatch cluster.

5.2 LargeOfficeNew load peak shaving dispatch

This section applies the analysis described in Figure (7) to the peak shaving dispatch profile simulated by QuESt for the "LargeOfficeNew" facility load.

5.2.1 Selection of number of clusters

Previous studies of residential facility load have revealed the differences in load between seasons [35]. As peak shaving dispatch is dependent on facility load, we conduct a seasonal analysis of the peak shaving dispatch to choose the number of clusters, k. We divide this dispatch into four seasonal events as follows:

(i) Spring: March, April, May
(ii) Summer: June, July, August
(iii) Fall: September, October, November
(iv) Winter: December, January, February

Figure (8) shows the histogram of peak shaving dispatch on the "LargeOfficeNew" load for each season. We find that a majority of dispatch occurs in the summer, with limited activity in the winter and roughly equivalent dispatch distribution in the spring and fall. We also evaluate the differences in charging across seasons. This is shown in Figure (9); there are only 19 charging instances during the winter season, while all other seasons have at least 80.

Based on the seasonal analysis, there appears to be an active dispatch segment of the year (summer), followed by a section of the year of moderate dispatch activity (spring and fall), and a section of mild dispatch (winter). We choose a value for k = 2 for k-means clustering, to cluster the dispatch between the active dispatch and the moderate/mild dispatch, and then characterize the duty cycle within each cluster.

5.1.2 Clustering analysis

Using the methodology for k-means described in Section 3.4 with k = 2, we obtain two clusters, Cluster 1 and Cluster 2. Figure

(10) is the assignment of clusters for each nonzero dispatch day throughout the year. Day assignments for Cluster 1 fall mainly in the summer, and day assignments for Cluster 2 fall mainly in the remainder of the year.

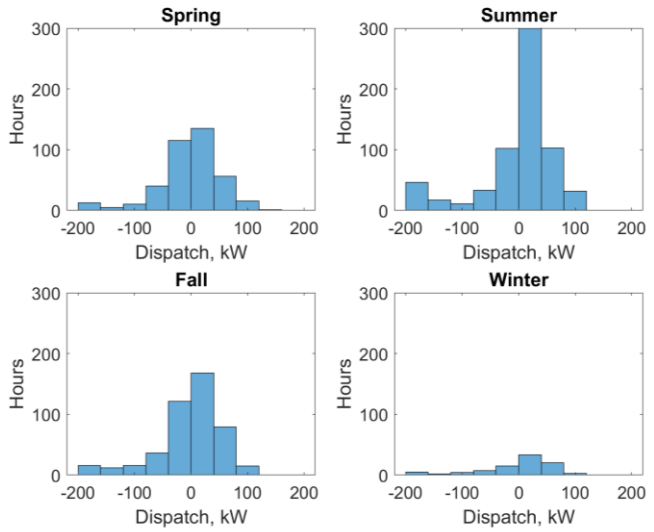

FIGURE 8: HISTOGRAM OF NONZERO PEAK SHAVING DISPATCH BY SEASON, "LARGEOFFICENEW".

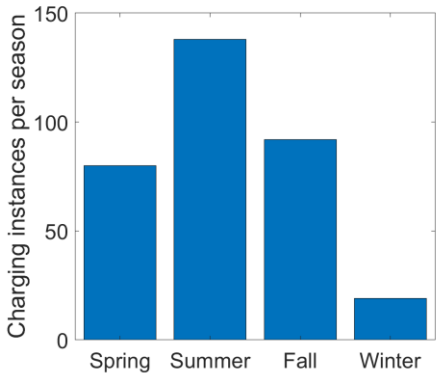

FIGURE 9: CHARGING INSTANCES BY SEASON, "LARGEOFFICENEW".

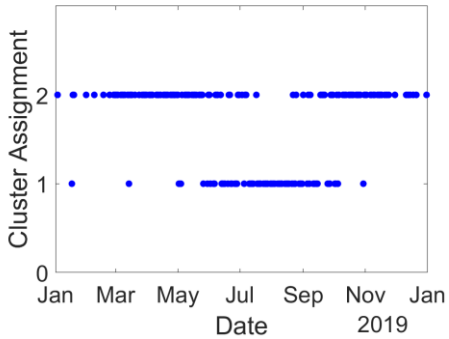

FIGURE 10: CLUSTER ASSIGNMENTS FOR EACH DAY OF YEARLY DISPATCH. "LARGEOFFICENEW". Days without charge or discharge (zero-dispatch days) are not assigned a cluster.

The two clusters have respective centroids, here interpreted as a representative daily dispatch of the battery within each cluster. Figure (11) shows the two cluster centroids, with Centroid 1 as the centroid for cluster 1, and Centroid 2 the centroid for cluster 2. It is from this figure that the underlying operating protocol for peak shaving dispatch in QuESt can be seen: the dispatch charges the battery immediately before the discharge required for peak shaving. As Centroid 1 requires a longer discharge at higher power than Centroid 2, the charging beforehand is at much higher power to fill the battery, in anticipation for a higher energy discharge.

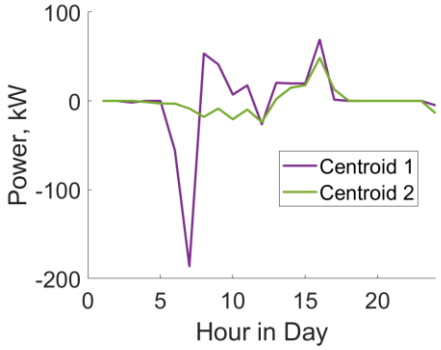

FIGURE 11: CLUSTER CENTROIDS OF YEARLY DISPATCH, "LARGEOFFICENEW". Cluster centroids as determined by k-means clustering on the yearly dispatch, cluster length 1 day = 24 hours.

We now compute the PSD for charge and discharge separately of the two clusters, with mean centering applied as described in Section 3.3. Figure (12) shows the PSD computed for charging and discharging for each cluster. The PSD as computed for Cluster 1 charging exhibits a strong peak at 4.123e-05 Hz, while the PSD as computed for Cluster 2 charging shows a much smaller peak at 2.279e-05 Hz. For discharging, the PSD as computed for Cluster 1 and Cluster 2 exhibit peaks of similar size, at 2.279e-05 Hz and 2.496e-05 Hz, respectively.

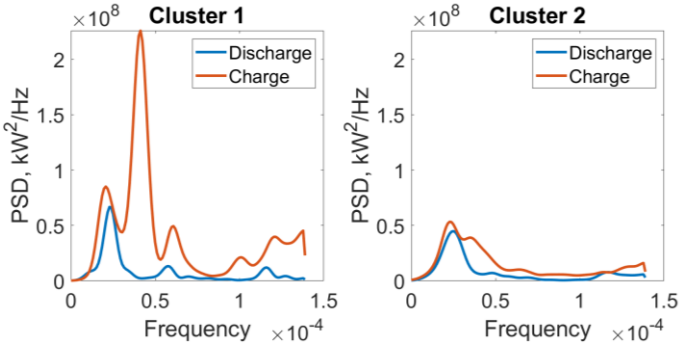

FIGURE 12: POWER SPECTRAL DENSITY OF PEAK SHAVING DISPATCH, "LARGEOFFICENEW", BY CLUSTER. PSD was conducted on clusters within the yearly dispatch, as assigned in Figure (10).

5.1.3 Comparison to PSD computed over entire dispatch

We also compute the PSD over the entire year without k-means clustering. This is presented in Figure (13). The PSD computed for charging contains a strong peak at 4.015e-5 Hz, and in the PSD computed for discharging, a peak at 2.387e-5 Hz. These are closer in value to those of Cluster 1, than those of Cluster 2. The PSD computed over the entire year is dominated by the charging profile in Cluster 1. However, Cluster 1 only represents 27% of the total nonzero dispatch days. Characterizing the peak-shaving dispatch duty cycle based on the yearly PSD would obscure the characteristic duty cycling of Cluster 2.

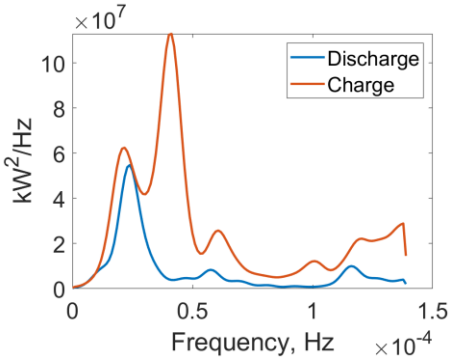

FIGURE 13: POWER SPECTRAL DENSITY OF PEAK SHAVING YEARLY DISPATCH, "LARGEOFFICENEW". The charging PSD exhibits a strong peak at 4.015e-5 Hz, while the discharging PSD exhibits a peak at 2.387e-5 Hz.

5.2 SuperMarketNew load peak shaving dispatch

This section applies the analysis described in Figure (7) to the peak shaving dispatch profile simulated by QuESt for the "SuperMarketNew" facility load, and compares the results of this analysis to that of the "LargeOfficeNew" facility load.

5.2.1 Selection of number of clusters

For the "SuperMarketNew" load, Figure (14) is the histogram for peak shaving dispatch profile on that load within each season, and Figure (15) is the instances of charging occurrences by season, displaying more consistent dispatch across seasons than for the "LargeOfficeNew" dispatch profile.

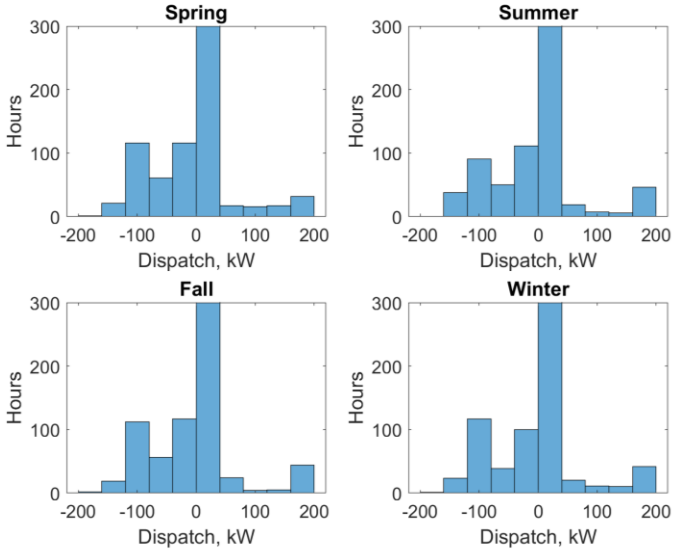

FIGURE 14: HISTOGRAM OF NONZERO PEAK SHAVING DISPATCH BY SEASON, "SUPERMARKETNEW".

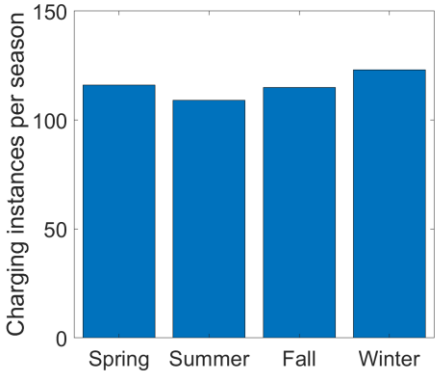

FIGURE 15: CHARGING INSTANCES BY SEASON, "SUPERMARKETNEW".

Unlike with the "LargeOfficeNew" dispatch profile, we cannot rely on seasonal differences in dispatch to inform the selection of number of clusters for the "SuperMarketNew" dispatch profile. We instead choose the number of clusters so that applying k-means clustering to the dispatch profile yields clusters of comparable sizes to avoid over-generalizing the dispatch and clustering the majority of daily dispatch into a given cluster. For this dispatch profile, using k = 2 yields one cluster with 344 days and one cluster with only 15 days. Using k = 3 yields three clusters of sizes 145, 113, and 101 days. We adopt this choice.

5.2.2. Clustering analysis

Using the methodology for k-means described in Section 4.3 with k = 3, we obtain three clusters, Cluster 1, Cluster 2, and Cluster 3. Figure (16) is the assignment of clusters for each nonzero dispatch day throughout the year. As expected from our

seasonal analysis on this dispatch profile, clusters do not appear to correspond to any seasonal dispatch.

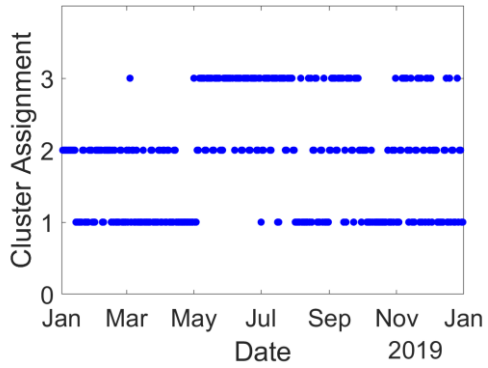

FIGURE 16: CLUSTER ASSIGNMENTS FOR EACH DAY OF YEARLY DISPATCH, "SUPERMARKETNEW". Days without charge and discharge (zero-dispatch days) are not assigned a cluster.

The three clusters have respective centroids, here interpreted as a representative daily dispatch of the battery within each cluster. Figure (17) shows the three cluster centroids, with Centroid 1 as the centroid for cluster 1, Centroid 2 as the centroid for cluster 2, and Centroid 3 the centroid for cluster 3. There are three distinct dispatch profiles: Centroid 1 represents days with a high charge power and low discharge power; Centroid 2 represents days with a low charge and discharge power; and Centroid 3 represents days with a high charge and discharge power.

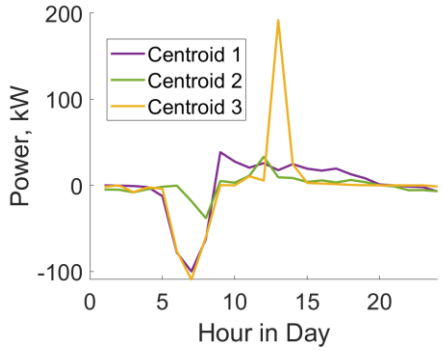

FIGURE 17: CLUSTER CENTROIDS OF YEARLY DISPATCH, "SUPERMARKETNEW". Cluster centroids as determined by k-means clustering on the yearly dispatch, cluster length 1 day = 24 hours.

The PSD for charge and discharge of the three clusters is computed, with mean centering applied as in Section 3.3. Figure (18) shows the PSD computed for charging and discharging for each cluster. Cluster 1 shows a strong peak in the PSD computed for charging, at 2.713e-5 Hz. Cluster 2 shows no discernable peaks in the PSD computed for charging and discharging. Cluster 3 shows peaks in the PSD computed for both charging and discharging, at 2.713e-5 Hz and 1.378e-4 Hz, respectively.

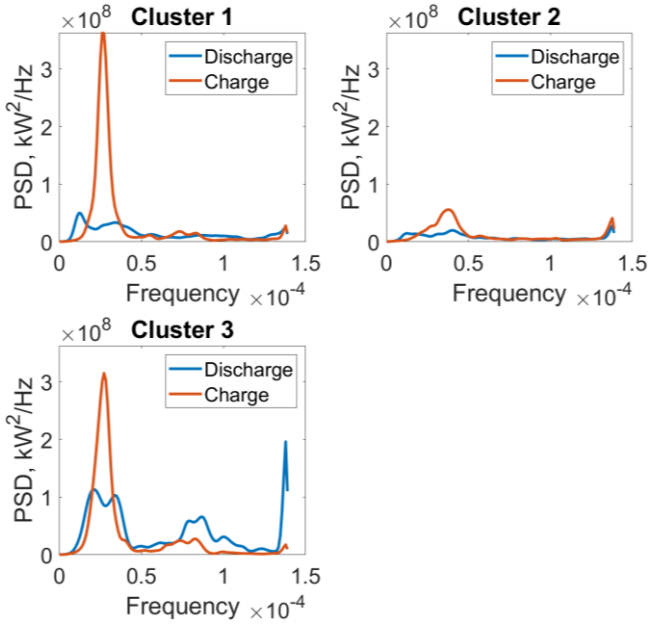

FIGURE 18: POWER SPECTRAL DENSITY OF PEAK SHAVING DISPATCH, "LARGEOFFICENEW", BY CLUSTER. PSD was conducted on clusters within the yearly dispatch, as assigned in Figure (16).

5.2.3. Comparison to PSD computed over entire dispatch

As in Section 5.1.3, we also compute the PSD over the entire year, without k-means clustering, for the "SuperMarketNew" dispatch profile. This is shown in Figure (19). The PSD computed for charging shows a peak at 2.604e-5 Hz, and no discernable peak for discharging. In this case, many of the duty cycling features present in the "SuperMarketNew" clusters are missing, including the large peak in the PSD computed for Cluster 3 discharging.

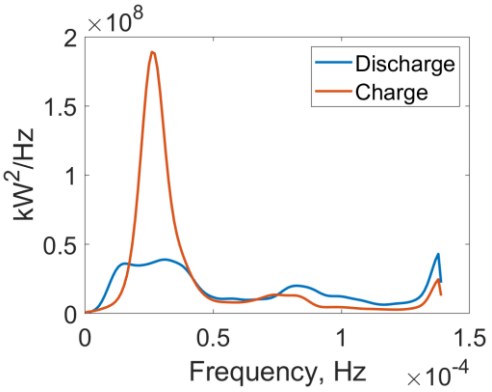

FIGURE 19: POWER SPECTRAL DENSITY OF PEAK SHAVING YEARLY DISPATCH, "SUPERMARKETNEW". The charging PSD exhibits a strong peak at 2.604e-5 Hz, while there is no discernable peak in discharge.

5.3. Comparison to electric vehicle duty cycles

Table (2) compares the frequency corresponding to the peak value of the PSD for peak shaving to those obtained by Z. Liu *et al.* in [13], which evaluated simulated 48V "mild-hybrid"

vehicle battery dispatch using PSD. These values are also compared to the same values obtained for the dispatch simulated of a Tesla Model S "fully-electric" vehicle battery, on the US06 and WLTP driving cycles. The "LargeOfficeNew" and "SuperMarketNew" yearly dispatches are chosen as representatives for peak shaving.

With the exception of the mild-hybrid vehicle discharge, the peak frequency of the PSD for peak shaving is at least two orders of magnitude smaller than that of the PSD for the batteries in automotive applications. Batteries for grid applications are excited across a different frequency range, and therefore exhibit different impedances, than in automotive applications. This difference has implications on the design of battery management systems (BMS) for grid batteries in comparison to electric automotive batteries, as BMS must be calibrated to account for the operating impedance range of the battery.

This difference also has implications on the operation of second-life batteries (i.e. post automotive-usage) for grid applications. As the second-life battery is excited across a different frequency range, its degradation within grid application operation will be different than in its "first-life" in electric vehicle operation. Therefore, any models to estimate degradation and capacity fade for the electric vehicle operation will no longer be accurate for the grid application operation, and new models must be constructed and calibrated for the new operation mode under grid application.

TABLE 2: PSD PEAK FREQUENCIES BY APPLICATION.

Application	Discharge PSD Peak Frequency, Hz	Charge PSD Peak Frequency, Hz
Peak Shaving, "LargeOfficeNew"	2.39e-5	4.02e-5
Peak Shaving, "SuperMarketNew"	2.60e-5	1.38e-4
Mild-Hybrid Vehicle [13]	4e-4 – 1.17e-2	3.52e-2 – 4.69e-2
Fully-Electric Vehicle, US06	7.81e-3	4.69e-2
Fully-Electric Vehicle, WLTP	1.56e-2	1.95e-2

6. CONCLUSIONS

A process for characterizing the duty cycle of grid applications for energy storage was presented, using k-means clustering and PSD to analyze the duty cycle of charge and discharge for stationary battery under peak shaving application. The duty cycle of peak shaving was compared to the duty cycle of a mild-hybrid vehicle battery and a fully-electric vehicle battery, showing distinct differences in frequency range between the duty cycles.

The combination of k-means clustering and PSD analysis captures features within each cluster, that would otherwise be lost in a PSD analysis conducted over the entire dispatch profile. This process also characterizes the variation in duty cycle within a peak shaving dispatch profile. This allows for direct comparison between peak shaving dispatch profiles, as well to other applications, such as batteries in mild-hybrid and fully-electric vehicle applications.

ACKNOWLEDGEMENTS

The research presented within this paper is supported by the Bits and Watts Initiative within the Precourt Institute for Energy at Stanford University.

REFERENCES

[1] IRENA, "Renewable capacity highlights," IRENA, Tech. Rep., 2020.

[2] NREL, "2018 renewable energy grid integration data book," U.S. Department of Energy, Tech. Rep., 2020, Available: https://www.nrel.gov/docs/fy20osti/74823.pdf.

[3] California ISO, "What the Duck Curve Tells us about Managing a Green Grid," California ISO, Tech. Rep., 2013, Available: https://www.caiso.com/Documents/FlexibleResourcesHelpRenewables_FastFacts.pdf.

[4] EIA, "U.S. battery storage market trends: May 2018," U.S. Energy Information Administration, Tech. Rep., 2018.

[5] Lazard, "Lazard's levelized cost of storage analysis - version 3.0," Lazard, Tech. Rep., 2017.

[6] T. Chen *et al.*, "Applications of Lithium-Ion Batteries in Grid-Scale Energy Storage Systems," *Transactions of Tianjin University,* pp. 1-10, 2020.

[7] Rocky Mountain Institute, "The Economics of Battery Energy Storage," Rocky Mountain Insitute, Tech. Rep., 2015, Available: https://rmi.org/insight/economics-battery-energy-storage/.

[8] F. Wankmüller *et al.*, "Impact of battery degradation on energy arbitrage revenue of grid-level energy storage," *Journal of Energy Storage,* vol. 10, pp. 56-66, 2017/04/01/ 2017, doi: https://doi.org/10.1016/j.est.2016.12.004.

[9] A. Stan, *et al.*, "Lithium ion battery chemistries from renewable energy storage to automotive and back-up power applications — An overview," in *2014 International Conference on Optimization of Electrical and Electronic Equipment (OPTIM)*, 22-24 May 2014 2014, pp. 713-720, doi: 10.1109/OPTIM.2014.6850936.

[10] A. J. Crawford *et al.*, "Lifecycle comparison of selected Li-ion battery chemistries under grid and electric vehicle duty cycle combinations," *Journal of Power Sources,* vol. 380, pp. 185-193, 2018.

[11] P. Spagnol, S. Onori, N. Madella, Y. Guezennec, and J. Neal, "Aging and characterization of li-ion batteries in a hev application for lifetime estimation," in *Proc. of IFAC Symposium Advances in Automotive Control*, 2010.

[12] W. Widanage *et al.*, "Design and use of multisine signals for Li-ion battery equivalent circuit modelling. Part 1: Signal

design," *Journal of Power Sources,* vol. 324, pp. 70-78, 2016.
[13] Z. Liu, S. Onori, and A. Ivanco, "Synthesis and experimental validation of battery aging test profiles based on real-world duty cycles for 48-V mild hybrid vehicles," *IEEE Transactions on Vehicular Technology,* vol. 66, no. 10, pp. 8702-8709, 2017.
[14] R. Mingant, J. Bernard, and V. Sauvant-Moynot, "Novel state-of-health diagnostic method for Li-ion battery in service," *Applied Energy,* vol. 183, pp. 390-398, 2016.
[15] Q. Kellner, *et al.*, "Duty-cycle characterisation of large-format automotive lithium ion pouch cells for high performance vehicle applications," *Journal of Energy Storage,* vol. 19, pp. 170-184, 2018.
[16] R. Zhu *et al.*, "Accurate lithium-ion battery modeling with inverse repeat binary sequence for electric vehicle applications," *Applied Energy,* vol. 251, p. 113339, 2019.
[17] D. R. Conover *et al.*, "Protocol for Uniformly Measuring and Expressing the Performance of Energy Storage Systems," United States, 2016-04-01 2016. [Online]. Available: https://www.osti.gov/servlets/purl/1249270
[18] D. A. Schoenwald and J. Ellison, "Determination of Duty Cycle for Energy Storage Systems in a PV Smoothing Application," United States, 2016-04-01 2016. [Online]. Available: https://www.osti.gov/servlets/purl/1331494
[19] D. Rosewater and S. Ferreira, "Development of a frequency regulation duty-cycle for standardized energy storage performance testing," (in English), 2016-05-25 2016, doi: 10.1016/j.est.2016.04.004.
[20] D. Stroe *et al.* "Operation of a Grid-Connected Lithium-Ion Battery Energy Storage System for Primary Frequency Regulation: A Battery Lifetime Perspective," *IEEE Transactions on Industry Applications,* vol. 53, no. 1, pp. 430-438, 2017, doi: 10.1109/TIA.2016.2616319.
[21] M. Uddin, *et al.*, "A review on peak load shaving strategies," *Renewable and Sustainable Energy Reviews,* vol. 82, pp. 3323-3332, 2018/02/01/ 2018, doi: https://doi.org/10.1016/j.rser.2017.10.056.
[22] "End-User Bill Management," *Energy Storage Association,* 2013, Available: https://energystorage.org/end-user-bill-management/.
[23] NREL, "Identifying Potential Markets for Behind-the-Meter Battery Energy Storage: A Survey of U.S. Demand Charges," U.S. Department of Energy, Tech. Rep., 2017, Available: https://www.nrel.gov/docs/fy17osti/68963.pdf.
[24] J. Leadbetter and L. Swan, "Battery storage system for residential electricity peak demand shaving," *Energy and Buildings,* vol. 55, pp. 685-692, 2012/12/01/ 2012, doi: https://doi.org/10.1016/j.enbuild.2012.09.035.
[25] E. Reihani, S. Sepasi, L. R. Roose, and M. Matsuura, "Energy management at the distribution grid using a Battery Energy Storage System (BESS)," *International Journal of Electrical Power & Energy Systems,* vol. 77, pp. 337-344, 2016/05/01/ 2016, doi: https://doi.org/10.1016/j.ijepes.2015.11.035.
[26] J. W. Cooley, P. A. W. Lewis, and P. D. Welch, "The Fast Fourier Transform and Its Applications," *IEEE Transactions on Education,* vol. 12, no. 1, pp. 27-34, 1969, doi: 10.1109/TE.1969.4320436.
[27] P. Welch, "The use of fast Fourier transform for the estimation of power spectra: A method based on time averaging over short, modified periodograms," *IEEE Transactions on Audio and Electroacoustics,* vol. 15, no. 2, pp. 70-73, 1967, doi: 10.1109/TAU.1967.1161901.
[28] Sandia National Labs, "PSD computations using Welch's method," U.S. Department of Energy, Tech. Rep., 1991, Available: https://www.osti.gov/biblio/5688766/.
[29] A. K. Jain, M. N. Murty, and P. J. Flynn, "Data clustering: a review," *ACM Comput. Surv.,* vol. 31, no. 3, pp. 264–323, 1999, doi: 10.1145/331499.331504.
[30] T. Warren Liao, "Clustering of time series data—a survey," *Pattern Recognition,* vol. 38, no. 11, pp. 1857-1874, 2005/11/01/ 2005, doi: https://doi.org/10.1016/j.patcog.2005.01.025.
[31] D. Arthur and S. Vassilvitskii, "k-means++: the advantages of careful seeding," presented at the Proceedings of the eighteenth annual ACM-SIAM symposium on Discrete algorithms, New Orleans, Louisiana, 2007.
[32] T. Xu and N. Zhang, "Coordinated Operation of Concentrated Solar Power and Wind Resources for the Provision of Energy and Reserve Services," *IEEE Transactions on Power Systems,* vol. 32, no. 2, pp. 1260-1271, 2017, doi: 10.1109/TPWRS.2016.2571561.
[33] S. R. Deeba, *et al.*, "A tool to estimate maximum arbitrage from battery energy storage by maintaining voltage limits in an LV network," in *2015 IEEE PES Asia-Pacific Power and Energy Engineering Conference (APPEEC)*, 15-18 Nov. 2015 2015, pp. 1-5, doi: 10.1109/APPEEC.2015.7380894.
[34] R. Green, I. Staffell, and N. Vasilakos, "Divide and Conquer? ${k}$-Means Clustering of Demand Data Allows Rapid and Accurate Simulations of the British Electricity System," *IEEE Transactions on Engineering Management,* vol. 61, no. 2, pp. 251-260, 2014, doi: 10.1109/TEM.2013.2284386.
[35] J. D. Rhodes *et al.*, "Clustering analysis of residential electricity demand profiles," *Applied Energy,* vol. 135, pp. 461-471, 2014/12/15/ 2014, doi: https://doi.org/10.1016/j.apenergy.2014.08.111.
[36] A. Devie, *et al.*, "Classification of duty pulses affecting energy storage systems in vehicular applications," in *2010 IEEE Vehicle Power and Propulsion Conference*, 1-3 Sept. 2010 2010, pp. 1-6, doi: 10.1109/VPPC.2010.5729137.
[37] Sandia National Labs, "QuESt: An Energy Storage Evaluation Application Suite," U.S. Department of Energy, 2018, Available: https://www.sandia.gov/ess-ssl/tools/quest/.